

RESEARCH ARTICLE | APRIL 09 2024

An algorithm to enhance the capability of imaging Thomson scattering

Yi-fan Liu ; Peng Yuan ; Tao Tao ; Yao-yuan Liu ; Xin-yan Li ; Jun Li ; Jian Zheng  



AIP Advances 14, 045313 (2024)

<https://doi.org/10.1063/5.0191058>



AIP Advances

Special Topic: Machine Vision, Optical Sensing and Measurement

Submit Today



An algorithm to enhance the capability of imaging Thomson scattering

Cite as: AIP Advances 14, 045313 (2024); doi: 10.1063/5.0191058

Submitted: 27 January 2024 • Accepted: 22 March 2024 •

Published Online: 9 April 2024



View Online



Export Citation



CrossMark

Yi-fan Liu,¹ Peng Yuan,^{1,a)} Tao Tao,¹ Yao-yuan Liu,¹ Xin-yan Li,¹ Jun Li,¹ and Jian Zheng^{1,2,b)}

AFFILIATIONS

¹Department of Plasma Physics and Fusion Engineering, University of Science and Technology of China, Hefei, Anhui 230027, People's Republic of China

²IFSA Collaborative Innovation Center, Shanghai Jiao Tong University, Shanghai 200240, People's Republic of China

^{a)}Electronic mail: yuanpeng@ustc.edu.cn

^{b)}Author to whom correspondence should be addressed: jzheng@ustc.edu.cn

ABSTRACT

Collective Thomson scattering (TS) is a powerful technique to accurately diagnose the parameters of laser-produced plasmas. However, when the scattering parameter α , which is inverse to the product of electron Debye length and wavenumber of plasma fluctuations, is significantly larger than 1, which of the conditions is easily satisfied in the experiment, the accuracy of electron density measurement is usually poor just with the single-wavenumber ion-acoustic wave feature of the TS spectrum. This situation can be greatly improved in the imaging TS experiment because the signal intensity is proportional to electron density. A novel algorithm is developed and validated for the data analysis of imaging TS through the combination of signal intensity and spectral profile. The results show that we can obtain the electron density with high confidence, as well as other plasma parameters like electron and ion temperatures.

© 2024 Author(s). All article content, except where otherwise noted, is licensed under a Creative Commons Attribution (CC BY) license (<http://creativecommons.org/licenses/by/4.0/>). <https://doi.org/10.1063/5.0191058>

I. INTRODUCTION

Collective Thomson scattering (TS) is one of the most powerful diagnostics of under-dense plasmas in the field of high-energy-density physics.^{1,2} With various experimental setups, time-integrated or time-resolved Thomson scattering spectra from different plasma positions are obtained, and plasma parameters are thus inferred.³⁻⁹ In the early experiments, the states of laser-produced plasmas at different spatial positions are usually measured shot-by-shot. In order to minimize the uncertainties due to shot-to-shot fluctuations, the imaging Thomson scattering (iTS) technique is developed,^{10,11} which is able to offer a space-resolved diagnosis of plasma parameters along the probe beam in a single laser shot. At present, iTS is widely used and has become a significant research method for numerous physical issues such as heat transportation,^{10,12-14} plasma shocks,^{15,16} ion species fraction,¹⁷ self-generated magnetic field,¹⁸ collisional absorption,¹⁹ etc.

In collective Thomson scattering diagnostics, plasma states are mainly inferred via fitting the spectra with theoretical ones.

When the scattering parameter, i.e., the reciprocal of the product of wave number and electron Debye length, is significantly larger than one, the ion-acoustic wave (IAW) feature of the spectrum weakly depends on electron density, leading to a large fitting uncertainty of electron density.²⁰ In order to enhance the measurement accuracy of electron density, one way is to detect the electron plasma wave feature of collective Thomson scattering. Unfortunately, for the coronal plasma in laser fusion, the scattered intensity of the electron plasma wave feature is two or three orders lower than that of the ion-acoustic feature¹ and, therefore, is easily corrupted with noises and stray signals. Hence, it is common practice to focus solely on the measurement of ion-acoustic features in many cases. Several methods are developed to improve measurement accuracy, such as absolute calibration by Rayleigh scattering,¹² dual-wavelength TS,²¹ and dual-angle TS.^{20,22}

Since iTS offers the dependence of signal intensity as well as spectral profile on spatial position along the probe beam and the signal intensity is proportional to electron density, it is natural to expect that electron density could be accurately inferred from the

iTS spectrum even if only ion-acoustic wave features are detected. In this article, we develop an algorithm to improve the retrieval accuracy of plasma parameters from ion-acoustic wave features of iTS by combining the spectral profile and intensity distribution. To our best knowledge, this is the first algorithm for iTS. In the fitting procedure, of course, preliminary knowledge of electron density distribution has to be assumed. It is a fortune that, in many cases, the electron density distribution is roughly known. For example, when a solid plate target is irradiated with a laser pulse, the spatial distributions of electron density along the target normal can be approximately described with an exponential²³ or double-exponential²⁴ function. With reasonable assumptions on the electron density distribution and the aid of radiation hydro simulation, we show that the fitting uncertainties of plasma parameters can be greatly improved with the newly developed algorithm, even in the region of scattering parameters significantly larger than one.

II. ALGORITHM AND VALIDATION

A. Algorithm

The Thomson scattered power spectrum from high-temperature plasmas is given by^{1,25}

$$P_s(\mathbf{k}, \omega) d\Omega d\omega_s = \frac{P_i r_0^2}{2\pi A} \left(1 + \frac{2\omega}{\omega_i}\right) |\hat{\mathbf{s}} \times (\hat{\mathbf{s}} \times \hat{\mathbf{E}}_{i0})|^2 N S(\mathbf{k}, \omega) d\Omega d\omega_s, \quad (1)$$

in which P_s and P_i are the scattered and incident power, respectively, r_0 is the classical electron radius, A is the cross-section area of the incident probe beam, $\omega = \omega_s - \omega_i$ is the frequency shift of the scattering wave, $\mathbf{k} = \mathbf{k}_s - \mathbf{k}_i$ is the differential wave vector, $\hat{\mathbf{s}}$ is the direction of scattered light, $\hat{\mathbf{E}}_{i0}$ is the polarization vector of the incident light, N is the electron number in the scattering volume, and $d\Omega$ is the solid angle of the collector. When considering the IAW component only, the relativistic correction term $2\omega/\omega_i$ in Eq. (1) could be neglected.

The profile of the scattered spectrum is dominated by the dynamic form factor $S(\mathbf{k}, \omega)$, which is the spectral intensity of the electron density auto-correlation function. In this article, the following formula is chosen for the dynamic form factor for the sake of simplicity:¹

$$S(\mathbf{k}, \omega) = \frac{1}{\sqrt{2\pi k v_e}} \left| 1 - \frac{\chi_e(\mathbf{k}, \omega)}{\epsilon(\mathbf{k}, \omega)} \right|^2 \exp\left(-\frac{\omega^2}{2k^2 v_e^2}\right) + \frac{Z}{\sqrt{2\pi k v_i}} \left| \frac{\chi_e(\mathbf{k}, \omega)}{\epsilon(\mathbf{k}, \omega)} \right|^2 \exp\left(-\frac{\omega^2}{2k^2 v_i^2}\right). \quad (2)$$

Here, a collisionless plasma in quasi-equilibrium is assumed, $\epsilon = 1 + \chi_e + \chi_i$ is the plasma permittivity, $\chi_{e,i}$ are the electron/ion susceptibilities, $v_{e,i}$ are the electron/ion thermal speeds, and Z is the ion charge state, which is equal to the nuclear charge for a fully ionized plasma. In this simplified model, the IAW part is determined by electron density n_e , electron temperature T_e , and ion temperature T_i . Plasma flow and related drift between electrons and ions can be included in Eq. (2) by adding Doppler shifts.

In an iTS experiment, the information obtained has two dimensions, one is frequency and the other is spatial position. For an experiment with a scattering angle of 90° (seen in Fig. 1),

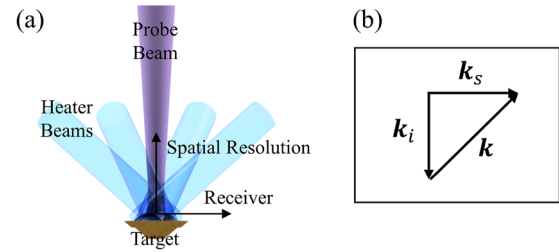


FIG. 1. (a) The configuration of Thomson scattering in simulation and (b) the scattering vector.

which means the differential wave vector \mathbf{k} is a constant, the scattered power could be written as a function of frequency ω_s and coordinate z ,

$$P_s(\omega_s, z) d\Omega d\omega_s = \frac{P_i r_0^2}{2\pi A} V n_e(z) S_i(\omega_s, z) d\Omega d\omega_s, \quad (3)$$

where V is the scattering volume, and S_i is the IAW part of the dynamic form factor. The scattered signal recorded by the detector is somewhat affected by the diagnostic system and can be described with the following equation:

$$I(\omega_s, z) = \kappa(z) R(\omega_s, z) [P_s(\omega_s, z) * F_\omega(\omega_s) * F_z(z)], \quad (4)$$

where κ is the absorption attenuation caused by the light passing through the plasma, R is the transmitting efficiency of the imaging system, and F_ω and F_z are the point-spread functions along the two dimensions. The content in the square bracket means that the signal received by the detector is the convolution of the scattered light and the point-spread functions. Since the spectral width of the IAW feature is narrow (around 1 nm) and the area to diagnose is small (within 2 mm), $R(\omega_s, z)$ is nearly constant and is unimportant to our method because it does not affect the shape of the spectra. F_ω and F_z can be determined by calibration. We assume that the absorption is fully due to the inverse bremsstrahlung absorption of the plasma,²⁶

$$\kappa_{ib} = \frac{16\pi Z n_e^2 e^6 \ln \Lambda}{3c v^2 (2\pi m_e T_e)^{3/2} (1 - n_e/n_c)^{1/2}}, \quad (5)$$

where $\ln \Lambda$ is the Coulomb logarithm, e is the electron charge, m_e is the electron mass, v is the frequency of the incident light, and n_c is the critical density corresponding to the probe. The intensity of the incident light decreases as $\kappa = e^{-\int \kappa_{ib} d\ell}$, where ℓ represents the path of light from the outermost point to the z point.

The spectral information, i.e., the information along the frequency dimension, is usually used to diagnose the plasma parameters in the previous research. Benefiting from the imaging method, the spatial distribution of the scattered intensity can also become a diagnostic basis. Integrating Eq. (4) over ω_s , we have

$$I(z) = \frac{P_i r_0^2}{2\pi A} \kappa(z) R(z) \{ [n_e(z) S_i(z)] * F_z(z) \}. \quad (6)$$

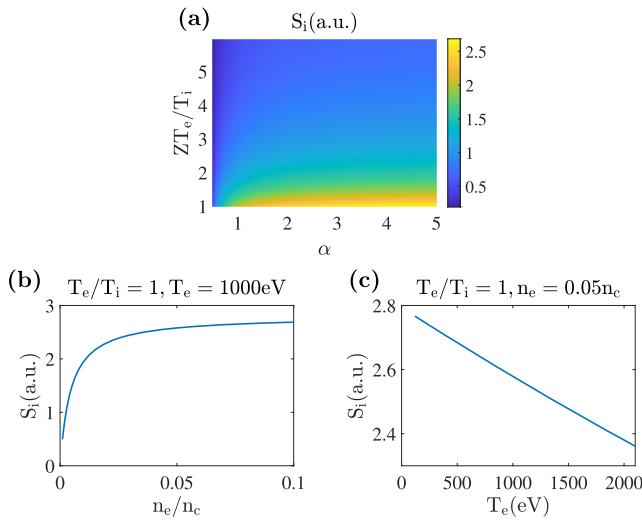


FIG. 2. (a) Pseudo-color image of spectrum-integral form factor as a function of scattering parameter α and quotient ZT_e/T_i for a fully ionized CH plasma. (b) Integral form factor as a function of electron density when $T_e = T_i = 1$ keV. (c) Integral form factor as a function of electron temperature when $n_e = 8 \times 10^{20} \text{cm}^{-3}$ and $T_e = T_i$.

Here, $S_i(z)$ is the spectrally integrated intensity of the IAW feature,

$$S_i(z) = \int_{\omega_i - 5\omega_{ia}/2}^{\omega_i + 5\omega_{ia}/2} S_i(z, \omega) d\omega, \quad (7)$$

where ω_{ia} is the frequency of the IAW, and $S_i(z)$ depends on spatial position through plasma parameters. We deem that the scattered energy is mainly concentrated within five times of the IAW frequency, as shown in Fig. 3(b). When the experimental system is set up, only n_e and S_i can affect the scattering intensity in Eq. (6). The dependence of $S_i(z)$ on plasma parameters is shown in Fig. 2. The critical density n_c is $1.608 \times 10^{22} \text{cm}^{-3}$ in this example, where the wavelength of the probe beam is 263 nm. S_i is nearly constant when electron density is higher than $0.05n_c$ at a given temperature, as seen

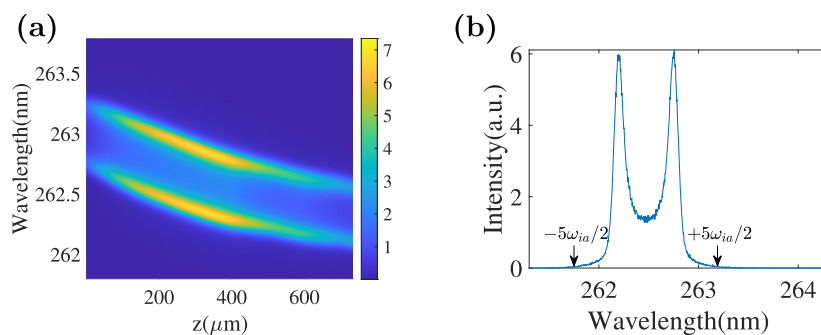


FIG. 3. (a) The synthetic spatial-resolved Thomson scattering spectra from ion-acoustic waves. (b) The scattered spectrum at $z = 400 \mu\text{m}$, where the electron density is $8.09 \times 10^{20} \text{cm}^{-3}$, the electron temperature is 886 eV, and the ion temperature is 784 eV. The corresponding positions of $\omega_i - 5\omega_{ia}/2$ and $\omega_i + 5\omega_{ia}/2$ are labeled by arrows.

in Fig. 2(b), but Fig. 2(c) shows that S_i is always sensitive to temperature in the range of values we consider. This is the reason why the fitting uncertainty of electron temperature could be small, but that of electron density is large. Another thing worth mentioning is that the nonlinear dependence of S_i on n_e is helpful to determine the absolute n_e .

In many experiments, the electron density distributions along the target normal have certain functional forms. After making reasonable assumptions about the spatial distribution function of electron density and represent $n_e(z)$ by several undetermined arguments, the scattering intensity curve can be fitted. Using the given electron density distribution, we can first fit the IAW spectra at different spatial points as usual and calculate the deviation between the fitting and experimental spectra by evaluating the chi-square value^{20,27}

$$\chi_1^2 = \frac{1}{N_z N_p} \sum_{i=1}^{N_z} \sum_{j=1}^{N_p} \frac{(s_{ij} - x_{ij})^2}{x_{ij}}, \quad (8)$$

where N_z is the number of spatial points, N_p is the number of pixels of the spectrum at each spatial position, s_{ij} is the count of the recorded spectrum at a given pixel of a recorder like a charge-coupled device, and x_{ij} is the corresponding value calculated by Eq. (4) using the fitting parameters. Under the current setting of $n_e(z)$, we figure out other parameters, including $T_e(z)$ and $T_i(z)$, that minimize the deviation. We also fit the scattered intensity distribution according to Eq. (6) and compute the chi-square value,

$$\chi_2^2 = \frac{1}{N_z} \sum_{i=1}^{N_z} \frac{(Y_i - y_i)^2}{y_i}, \quad (9)$$

where Y_i is the spectral-integrated intensity of scattered light at each spatial position, and y_i is the corresponding value calculated by Eq. (6) with the plasma parameters obtained in the previous step. χ_2^2 is sensitive to $n_e(z)$. Since we want to accurately infer electron density from the spectrally integrated intensity, a function χ^2 containing both χ_1 and χ_2 is needed as a key factor to combine the two steps (the specific form will be discussed in Sec. II B). Obviously,

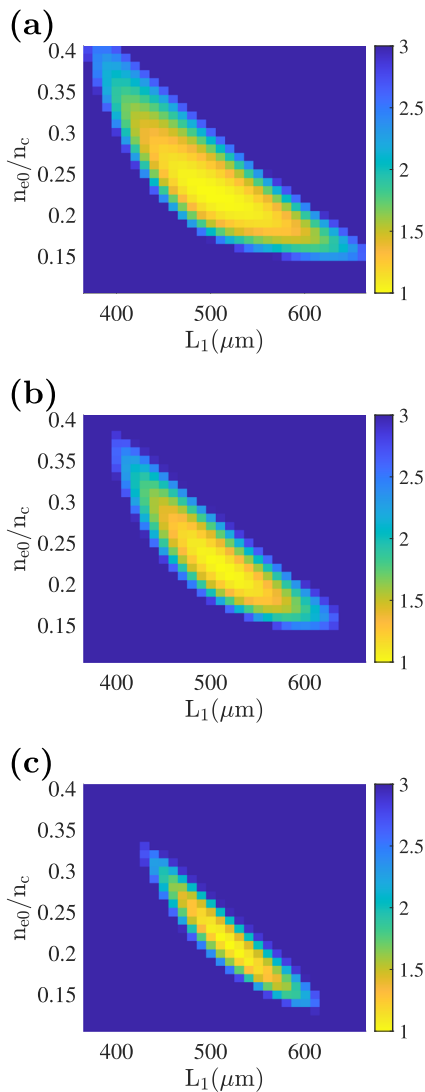


FIG. 4. The chi-square values (a) $\chi_1^2 + \chi_2^2$, (b) $(\chi_1 + \chi_2)^2$, and (c) $\chi_1\chi_2$ vs the first two arguments in the fitting of the synthetic spectra show that the smaller the value, the less deviation there is between the spectra and the fitting data. The values are normalized from the minimum.

χ^2 depends on the plasma parameters and their spatial distributions. The smaller the value, the less deviation there is between the experiment result and the fitting data. The set of arguments that minimizes χ^2 is selected as the final result. Therefore, $n_e(z)$ is determined, and other plasma parameters are also obtained in the process of fitting.

B. Numerical validation

We perform a numerical experiment to validate our method. With the radiation-hydrodynamic simulation code FLASH,²⁸ we simulate laser ablation processes relevant to the actual experiment²⁹ and generate a synthetic iTS graph of IAW. A probe beam at a

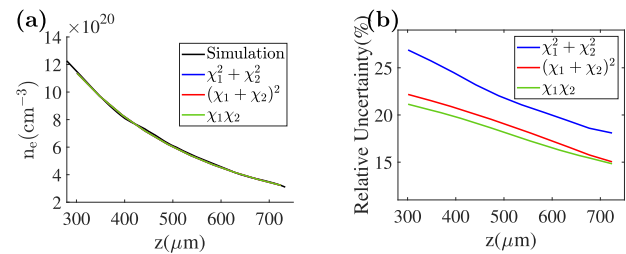


FIG. 5. The comparison of the three forms of χ^2 in terms of (a) diagnostic results and (b) fitting uncertainty of electron density.

wavelength of 263 nm (4ω) with an energy of 60 J is used for Thomson scattering. The probe beam has a 100 μm focal diameter and a pulse length of 3.5 ns. Four 1500 J heater beams at 351 nm (4ω) irradiate a spherical crown plastic target uniformly for 2.5 ns while the probe beam enters along the normal direction of the target, as shown in Fig. 1(a). The wave vectors of incident light, scattered light, and ion acoustic waves are illustrated in Fig. 1(b). A typical synthetic iTS graph is shown in Fig. 3(a), where the coordinate z denotes the distance from the target surface. A spectral resolution of 0.7 \AA and a spatial resolution of 90 μm are convolved, and a white noise with a standard deviation of 20% is added to the spectra via the Monte Carlo method. We treat the artificial data as an experimental result.

We assume that the electron density obeys a double exponential distribution along the z axis,²⁴

$$n_e(z) = n_{e0} \left[A e^{-z/L_1} + (1 - A) e^{-z/L_2} \right], \quad (10)$$

where z is the distance from the target, and n_{e0} , L_1 , L_2 , and A are four adjustable arguments to be determined. The rationality of the assumption will be proven by the fitting result. We analyze the iTS graph according to the method described in Sec. II A. The *collisionless and quasi-thermal equilibrium* dynamic form factor of Eq. (2) is adopted for the sake of simplification, which may not be proper in a real experiment. In order to reduce the potential error caused by absorption, the spatial range where intense absorption could occur is avoided in the fitting. Following the method mentioned in Sec. II A, we fit both the IAW spectra and the intensity distribution using the presupposed electron density and obtain χ_1 and χ_2 . To find an appropriate way to combine χ_1 and χ_2 , we have compared three homogeneous functional forms of χ^2 : $\chi_1^2 + \chi_2^2$, $(\chi_1 + \chi_2)^2$, and $\chi_1\chi_2$. Figures 4(a)–4(c) show the dependence of χ^2 values on the two fitting parameters. We take two times the minimum χ^2 as a boundary, and the value ranges of the electron density corresponding to the four fitting arguments within the boundary are taken as fitting uncertainty. As seen in the figure, although the definition of χ is different, the convergence region is similar. The fitting results with different definitions of χ are almost the same [see Fig. 5(a)]. However, the fitting uncertainties are notably different from each other [see Fig. 5(b)]. Therefore, we finally take $\chi_1\chi_2$ as a key evaluation factor because it turns out to have the fastest convergence rate. Figure 6 illustrates the entire fitting process.

Besides electron density, other plasma parameters are also calculated in the process of fitting the IAW spectra. The comparisons

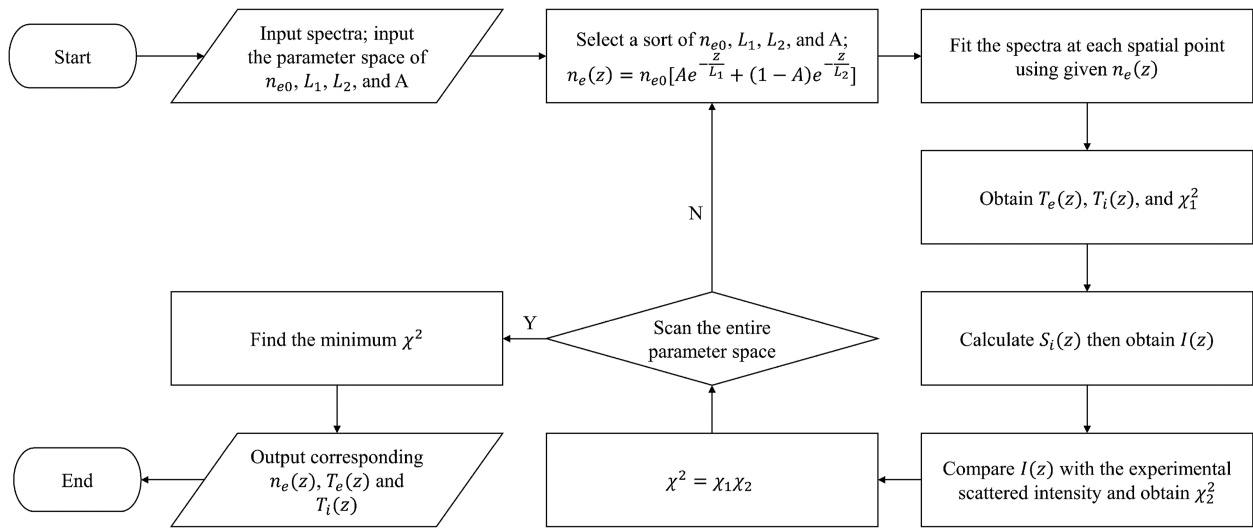


FIG. 6. The flow chart of the complete fitting process.

between the inferred results and the simulation values are shown in Figs. 7(a)–7(c). As seen in this figure, the inferred plasma parameters are in excellent agreement with the results from hydro simulations, which reveals that the model of Eq. (10) is reasonable. Figure 7(d) shows the scattering parameter α calculated with the plasma parameters of the simulation. Notice that the fitting uncertainty of T_e is smaller when α is larger and becomes greater with the decrease of α , although the uncertainty of n_e is smaller. For example, comparing the fitting results at $z = 300$ and $700 \mu\text{m}$, the uncertainty of n_e varies from 22 to 15%, while that of T_e varies from 1.1 to 2.3%. As revealed in the introduction, when the scattering parameter α is much larger than 1, the separation of two resonance peaks in the IAW spectrum is almost only dependent on temperature, and as α decreases, the influence of n_e gradually becomes significant. If we just fit the IAW spectra at each spatial point, the precision will be very poor, as shown in Figs. 7(a)–7(c). The error bars of dot-fitting are calculated in a similar way, where χ^2 is treated as a function of n_e , T_e , and T_i at each spatial point. The numerical experiment indicates that our algorithm can be applied to laser-plasma diagnostics and improve both precision and uncertainty with the IAW component of iTS. Because we are dealing with solid targets, we take the double-exponential function as the prior electron density distribution. We believe that in other cases, as long as the appropriate density distribution form is selected, the diagnostic accuracy can also be improved.

Figures 7(b) and 7(c) show that the fitting uncertainties of electron and ion temperatures are surprisingly low, which may be attributed to our using exactly the same Thomson scattering model in both generating and analyzing the spectra. There are several factors that might distort the signal in real experiments:

- (1) The effect of non-Maxwellian distribution and collision. It is worth pointing out that the scattering model we use is collisionless and quasi-thermal equilibrium. When

the heating beams keep irradiating, the TS spectra near the target exhibit abnormal shapes. With strong inverse bremsstrahlung heating and thermal conduction, the electron distribution function may significantly deviate from quasi-thermal equilibrium,³⁰ rendering our Thomson scattering model unsuitable.^{31,32} Recently, many theoretical^{33,34} and experimental³⁵ works about the collective Thomson scattering of non-equilibrium plasma have been carried out. It is necessary to modify the model when diagnosing plasmas in regions with large gradients.

- (2) The effect of absorption. The absorption effect will influence the intensity distribution. Although we take the absorption of incident light into account in Eq. (4), the absorption rate of the scattered light when it leaves plasma is unknown because we do not diagnose the lateral distribution of the plasma parameters. Under ideal circumstances, we can use Gaussian density and constant temperature to estimate the lateral properties. However, in more general cases, we recommend lowering the absorption rate with a higher-frequency probe and analyzing areas where the absorption is not obvious.
- (3) Errors in signal acquisition. Noises can introduce errors in the calculation of the scattered intensity. The uniform background (like bremsstrahlung) can be easily figured out from the area without signal, so what is important is to shield irrelevant signals like stray lights in the optical path.

Here we choose the double-exponential function as the expression for $n_e(z)$ because predecessors' research shows that this function can well describe $n_e(z)$ in the condition of a spherical crown target. Figure 8 shows the fitting result of $n_e(z)$ under different assumptive expressions, including exponential, double-exponential, and triple-exponential (adding one more exponential term). The result of the exponential distribution indicates that an improper

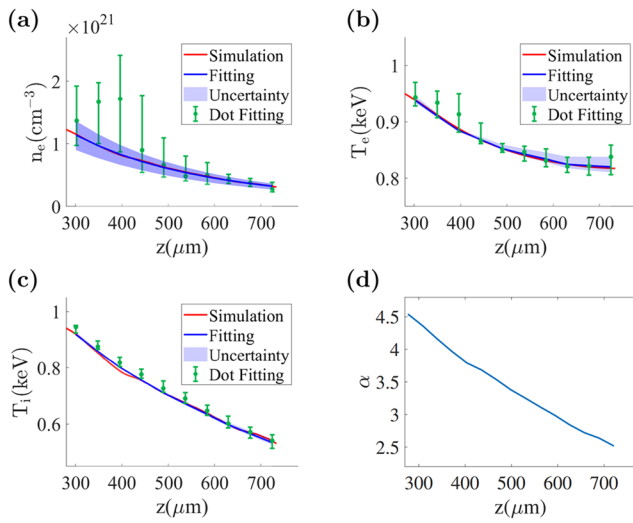


FIG. 7. The (a) electron density, (b) electron temperature, and (c) ion temperature calculated via our statistical fitting method (blue lines) and fitting at each space point (green dots) are compared to the original simulation results. We also present (d) the spatial distribution of the scattering parameter α as a reference for the fitting uncertainty.

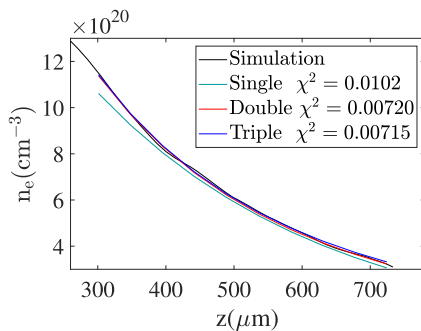


FIG. 8. The diagnostic results of different pre-determined analytical expressions of $n_e(z)$, including exponential (green), double-exponential (red), and triple-exponential (blue) functions.

assumption will lead to a large deviation. We believe that our analysis method can be applied to other configurations as long as the appropriate forms of $n_e(z)$ are selected. If a diagnosis under some new configuration is needed and the form of $n_e(z)$ is unknown, we think asymptotic approximation by a system of functions is feasible. The fitting results as well as the convergent χ^2 values of double-exponential and triple-exponential distributions are similar, as shown in Fig. 8, indicating that the first few terms are sufficient to describe n_e for a suitable function system. The selection of the system of functions can be roughly judged from the integral scattering intensity distribution curve because it is strongly dependent on $n_e(z)$. Besides, radiation-hydrodynamic simulation also has guiding significance.

III. CONCLUSION

Based on the imaging Thomson scattering (iTS) technique, we develop a novel data processing algorithm. Taking into account the spatial distribution information of the scattered light intensity, we propose a solution to the quest for electron density diagnostics with only an imaged IAW scattered component. The algorithm is validated by fitting synthetic Thomson scattering data generated from radiation hydrodynamic simulations. The fitting uncertainty of electron density is around 20%, and that of electron temperature is within 3%. Compared with the method of fitting IAW spectra point by point, the novel algorithm can be applied to infer plasma parameters with much lower uncertainties and, therefore, should be useful to analyze iTS results to accurately and reliably obtain the spatial distributions of plasma parameters.

ACKNOWLEDGMENTS

This work was supported by the Strategic Priority Research Program of the Chinese Academy of Sciences (Grant No. XDA25010200) and the National Key R&D Project (Grant No. 2023YFA160005602).

AUTHOR DECLARATIONS

Conflict of Interest

The authors have no conflicts to disclose.

Author Contributions

Yi-fan Liu: Conceptualization (equal); Data curation (equal); Formal analysis (equal); Investigation (equal); Methodology (equal); Software (equal); Validation (equal); Visualization (equal); Writing – original draft (equal); Writing – review & editing (equal). **Peng Yuan:** Conceptualization (equal); Data curation (equal); Investigation (lead); Methodology (equal); Visualization (supporting); Writing – review & editing (supporting). **Tao Tao:** Formal analysis (equal); Investigation (equal); Software (equal). **Yao-yuan Liu:** Conceptualization (equal); Methodology (supporting); Software (lead). **Xin-yan Li:** Data curation (supporting); Investigation (equal). **Jun Li:** Funding acquisition (equal); Writing – review & editing (equal). **Jian Zheng:** Conceptualization (equal); Funding acquisition (lead); Methodology (equal); Project administration (lead); Resources (lead); Software (lead); Validation (equal); Writing – original draft (equal); Writing – review & editing (supporting).

DATA AVAILABILITY

The data that support the findings of this study are available from the corresponding author upon reasonable request.

REFERENCES

- D. H. Froula, S. H. Glenzer, N. C. Luhmann, and J. Sheffield, *Plasma Scattering of Electromagnetic Radiation* (Academic Press, New York, 2011).
- S. S. Harilal, M. C. Phillips, D. H. Froula, K. K. Anoop, R. C. Issac, and F. N. Beg, *Rev. Mod. Phys.* **94**, 035002 (2022).

- ³S. M. Cameron, M. D. Tracy, K. G. Estabrook, and J. S. DeGroot, *Rev. Sci. Instrum.* **63**, 5259 (1992).
- ⁴B. L. Fontaine, H. A. Baldis, D. M. Villeneuve, J. Dunn, G. D. Enright, J. C. Kieffer, H. Pépin, M. D. Rosen, D. L. Matthews, and S. Maxon, *Phys. Plasmas* **1**, 2329 (1994).
- ⁵S. H. Glenzer, C. A. Back, K. G. Estabrook, and B. J. MacGowan, *Rev. Sci. Instrum.* **68**, 668 (1997).
- ⁶S. H. Glenzer, C. A. Back, L. J. Suter, M. A. Blain, O. L. Landen, J. D. Lindl, B. J. MacGowan, G. F. Stone, R. E. Turner, and B. H. Wilde, *Phys. Rev. Lett.* **79**, 1277 (1997).
- ⁷B. Bai, J. Zheng, W. Liu, C. X. Yu, X. Jiang, X. Yuan, W. Li, and Z. J. Zheng, *Phys. Plasmas* **8**, 4144 (2001).
- ⁸Z. Wang, J. Zheng, B. Zhao, C. X. Yu, X. Jiang, W. Li, S. Liu, Y. Ding, and Z. Zheng, *Phys. Plasmas* **12**, 082703 (2005).
- ⁹J. S. Ross, S. H. Glenzer, J. P. Palastro, B. B. Pollock, D. Price, L. Divol, G. R. Tynan, and D. H. Froula, *Phys. Rev. Lett.* **104**, 105001 (2010).
- ¹⁰F. Amiranoff, S. D. Baton, S. Hüller, V. Malka, A. Modena, P. Mounaix, N. R.-L. Galloudec, C. Rousseaux, and M. Salvati, *Phys. Rev. E* **61**, 1949 (2000).
- ¹¹J. S. Ross, D. H. Froula, A. J. Mackinnon, C. Sorce, N. Meezan, S. H. Glenzer, W. Armstrong, R. Bahr, R. Huff, and K. Thorp, *Rev. Sci. Instrum.* **77**, 10E520 (2006).
- ¹²G. Gregori, S. H. Glenzer, J. Knight, C. Niemann, D. Price, D. H. Froula, M. J. Edwards, R. P. J. Town, A. Brantov, W. Rozmus, and V. Y. Bychenkov, *Phys. Rev. Lett.* **92**, 205006 (2004).
- ¹³D. H. Froula, J. S. Ross, B. B. Pollock, P. Davis, A. N. James, L. Divol, M. J. Edwards, A. A. Offenberger, D. Price, R. P. J. Town, G. R. Tynan, and S. H. Glenzer, *Phys. Rev. Lett.* **98**, 135001 (2007).
- ¹⁴R. J. Henchen, M. Sherlock, W. Rozmus, J. Katz, P. E. Masson-Laborde, D. Cao, J. P. Palastro, and D. H. Froula, *Phys. Plasmas* **26**, 032104 (2019).
- ¹⁵T. Morita, Y. Sakawa, K. Tomita, T. Ide, Y. Kuramitsu, K. Nishio, K. Nakayama, K. Inoue, T. Moritaka, H. Ide, M. Kuwada, K. Tsubouchi, K. Uchino, and H. Takabe, *Phys. Plasmas* **20**, 092115 (2013).
- ¹⁶H. G. Rinderknecht, H.-S. Park, J. S. Ross, P. A. Amendt, D. P. Higginson, S. C. Wilks, D. Haberberger, J. Katz, D. H. Froula, N. M. Hoffman, G. Kagan, B. D. Keenan, and E. L. Vold, *Phys. Rev. Lett.* **120**, 095001 (2018).
- ¹⁷J. S. Ross, H.-S. Park, P. Amendt, L. Divol, N. L. Kugland, W. Rozmus, and S. H. Glenzer, *Rev. Sci. Instrum.* **83**, 10E323 (2012).
- ¹⁸R. Yamazaki, S. Matsukiyo, T. Morita, S. J. Tanaka, T. Umeda, K. Aihara, M. Edamoto, S. Egashira, R. Hatsuyama, T. Higuchi, T. Hihara, Y. Horie, M. Hoshino, A. Ishii, N. Ishizaka, Y. Itadani, T. Izumi, S. Kambayashi, S. Kakuchi, N. Katsuki, R. Kawamura, Y. Kawamura, S. Kisaka, T. Kojima, A. Konuma, R. Kumar, T. Minami, I. Miyata, T. Moritaka, Y. Murakami, K. Nagashima, Y. Nakagawa, T. Nishimoto, Y. Nishioka, Y. Ohira, N. Ohnishi, M. Ota, N. Ozaki, T. Sano, K. Sakai, S. Sei, J. Shiota, Y. Shoji, K. Sugiyama, D. Suzuki, M. Takagi, H. Toda, S. Tomita, S. Tomiya, H. Yoneda, T. Takezaki, K. Tomita, Y. Kuramitsu, and Y. Sakawa, *Phys. Rev. E* **105**, 025203 (2022).
- ¹⁹D. Turnbull, J. Katz, M. Sherlock, L. Divol, N. R. Shaffer, D. J. Strozzi, A. Colaitis, D. H. Edgell, R. K. Follett, K. R. McMillen, P. Michel, A. L. Milder, and D. H. Froula, *Phys. Rev. Lett.* **130**, 145103 (2023).
- ²⁰Y. Liu, Y. Ding, and J. Zheng, *Rev. Sci. Instrum.* **90**, 083501 (2019).
- ²¹D. H. Froula, P. Davis, L. Divol, J. S. Ross, N. Meezan, D. Price, S. H. Glenzer, and C. Rousseaux, *Phys. Rev. Lett.* **95**, 195005 (2005).
- ²²W.-q. Tan, Y.-y. Liu, X.-y. Li, P. Yuan, H. Zhao, Z.-c. Li, and J. Zheng, *J. Appl. Phys.* **129**, 043302 (2021).
- ²³R. Fabbro, C. Max, and E. Fabre, *Phys. Fluids* **28**, 1463 (1985).
- ²⁴D. Haberberger, S. Ivancic, S. X. Hu, R. Boni, M. Barczys, R. S. Craxton, and D. H. Froula, *Phys. Plasmas* **21**, 056304 (2014).
- ²⁵J. Zheng and C. X. Yu, *Plasma Phys. Controlled Fusion* **51**, 095009 (2009).
- ²⁶T. W. Johnston and J. M. Dawson, *Phys. Fluids* **16**, 722 (1973).
- ²⁷P. F. Knapp and W. E. Lewis, *Rev. Sci. Instrum.* **94**, 061103 (2023).
- ²⁸B. Fryxell, K. Olson, P. Ricker, F. X. Timmes, M. Zingale, D. Q. Lamb, P. MacNeice, R. Rosner, J. W. Truran, and H. Tufo, *Astrophys. J., Suppl. Ser.* **131**, 273 (2000).
- ²⁹T. Tao, G. Zheng, Q. Jia, R. Yan, and J. Zheng, *High Power Laser Sci. Eng.* **11**, e41 (2023).
- ³⁰A. B. Langdon, *Phys. Rev. Lett.* **44**, 575 (1980).
- ³¹J. Zheng, C. X. Yu, and Z. J. Zheng, *Phys. Plasmas* **4**, 2736 (1997).
- ³²Z. J. Liu, J. Zheng, and C. X. Yu, *Phys. Plasmas* **9**, 1073 (2002).
- ³³V. V. Belyi, *Phys. Rev. E* **97**, 053204 (2018).
- ³⁴A. L. Milder, S. T. Ivancic, J. P. Palastro, and D. H. Froula, *Phys. Plasmas* **26**, 022711 (2019).
- ³⁵R. J. Henchen, M. Sherlock, W. Rozmus, J. Katz, D. Cao, J. P. Palastro, and D. H. Froula, *Phys. Rev. Lett.* **121**, 125001 (2018).